**Online Publication Date: 20 December, 2011**

**Publisher: Asian Economic and Social Society**


# The effect of Hubbard potential on effective mass of carriers in doped Indium oxide

**Rahnamaye Aliabad H. A** ( Department of Physics, Sabzevar Tarbiat Moallem University, Sabzevar, Iran)

**Arabshahi H** (Department of Physics, Payame Noor University, P. O. Box 19395-3697, Tehran, Iran)

**Citation:** Rahnamaye Aliabad H. A, Arabshahi H (2011): "The effect of Hubbard potential on effective mass of carriers in doped Indium oxide " Journal of Asian Scientific Research , Vol.1, No.8,pp.427-440.

*Journal of Asian Scientific Research, Vol.1 (8), pp.427-440*

# The effect of Hubbard potential on effective mass of carriers in doped Indium oxide

**Author (s)**

**Rahnamaye Aliabad H. A**
Department of Physics,Sabzevar Tarbiat Moalem University, Sabzevar, Iran .

**Arabshahi H.**
Corresponding author, Department of Physics,Payame Noor University, Tehran, Iran.
E-mail: arabshahi@um.ac.ir

## Abstract

Structural and electronic properties of pure $In_2O_3$ and its alloys with Sc, Y, La and Ac including the band gap, the effective mass and the effect of dopant ionic radius have been investigated using density functional theory (DFT). The full potential linearized augmented plane wave (FL-LAPW) method was used with the local density approximation (LDA+*U*). The calculated results indicated that substituting indium atoms by these dopants have a significant influence on the structural and electronic properties of alloyed $In_2O_3$ crystals. Lattice parameters expand as a function of dopant ionic radii in the order Sc (9.987Å) < In (10.057Å) < Y (10.187Å) < La (10.446 Å) < Ac (10.546 Å) except for Sc dopant Sc (9.987Å) that shrinks. The band gap is increased with Sc and Y dopant while with Ac and La dopants decreases. The calculations have indicated that there are two band gaps for $In_2O_3$. One with a strong optical absorption, as direct band gap occurs from 0.81eV energy level below the top of valence band. The second is a much weaker absorption from top of the valence to the bottom of conduction band. The value of the electron effective mass in the bottom of conduction bands is increased for alloys $In_2O_3$. The results show that In *5s* states do not have significant hybridization with Sc *4s*, Y *5s*, La *6s* and Ac *7s* states.

## Introduction

Transparent Conducting Oxides (TCOs) materials have many applications in numerous devices such as flat panel displays, solar cells, gas sensors and low-emissive windows (Coutts et al., 1999; Ginley et al., 2000) Among various transparent oxides the indium tin oxide (ITO), indium oxide ($In_2O_3$), tin oxide ($SnO_2$), and zinc oxide (ZnO) are the dominant TCOs. Tin-doped indium oxide (ITO), with a typical electrical conductivity and transparency in the visible region is usually used in thin coating form. The development of polycrystalline or amorphous transparent conducting oxide (TCO) semiconductors used for practical thin-film transparent electrode applications are also have been discussed in the literature during the last few years (Minami, 2005; Lewis et al., 2000). Amorphous oxides have high electrical properties so that these properties are comparable with their crystalline phases. In amorphous compounds, there are not any crystalline nature and symmetry; therefore atoms have dangling bonds in any point of crystal. For example, in Si as a covalent material, the dangling bond states act as both electron and hole traps, since they are located at the center of the band gap. Therefore electronically properties of this compound show that amorphous behavior of this element is increase electrical resistance, in comparison with the crystalline nature (Mott, 1987). There are several drawbacks that could affect its future applicability. First, because of its relatively low conductivity it is not suitable for large-area displays. Second, it is not suitable for many full-color displays since it has a large optical absorption in the blue-green region (Ginley et al., 2005; Phillips et al., 1995). Third, in certain device structures in which ITO have been used there is lack of chemical instability e.g. organic light-emitting diodes. Regarding the thin film structure of TCO there are many attempts to find alternatives for these materials which are less expensive and possess comparable or higher conductivity (Ott et al., 1999; Coutts et al., 2000 ). Recently Takeo Ohsawa et al. (Ohsawa et al., 2011) show that, $Nb_{12}O_{29}$ film has transparent conducting properties with lowest resistivity of $3.3 \times 10^{-3}$ Ω·cm at room temperature. High transmittance (~70% at wavelength of 435 nm and ~50% at wavelength of 730 nm, 120 nm in thickness) in the visible is maintained with an optical band gap of ~ 4.0 eV. Their results show, the optical dielectric constant and effective mass were both larger than those for conventional transparent conducting oxides, leading $Nb_{12}O_{29}$ to exhibit high transparency.

Also, M. A. Noginov et al. (Lo et al., 2011) show that despite of low loss, silver and gold are not

suitable for a variety of nanoplasmonic applications in the infrared range, which require compact modes in single-interface plasmonic waveguides (Matsuishi et al., 2003). At the same time, degenerate wide-band-gap semiconductors can serve as high-quality plasmonic materials at telecom wavelengths, combining fairly high compactness and relatively low loss. Their plasmonic properties in the near-infrared can be compared to those of gold in the visible range. Obtained results by Shih-Shou Lo et al. (Lo et al., 2011) show a new transparent conductive oxide (TCO) layer with a monolayer of closed-pack Al-doped ZnO (AZO) spheres partly embedded in an AZO thin film. The average transmittance ratio in the wavelength range of 380–800 nm achieves 65% and 55%, respectively, when AZO spheres with a diameter of 500 nm are embedded in a thickness of 240 nm AZO thin films.

In this article we study the effect of substitutions Sc, Y, La and Ac on structural, the lattice parameter, the atomic positions, the band gap and the mobility of the carriers. Moreover, the effect of dopant ionic radius on the electronic structure of $In_2O_3$-based TCO has been investigated in the order: Sc (0.885 Å) < Y (1.04 Å) < La (1.172 Å) < Ac (1.260 Å). The heavily n-doped of $In_2O_3$ gives raise to a band-gap narrowing which is a consequence of many body effects on the conduction band. Alternatively, the band gap can also be altered by the local strains induced by the impurities. Local strains are able to change lattice parameters, therefore with changing volume, energy of lattice alter. So that, band gap of these compounds can be altering (Hayashi et al., 2005). A comparison of the structural, optical and electronic properties of the recently discovered nanoporous $Ca_{12}Al_{14}O_{33}$ TCO (Sushko et al., 2006 and 2007; Kajihara et al., 2007), with those of the conventional TCOs (such as Sc-doped CdO) is given by J. E Medvedeva and A. J. Freeman (Medvedeva et al., 2005), which indicates that this material belongs conceptually to a new class of transparent conductors.

The LDA method does not properly describe strongly correlated systems such as transition metal oxides or rare-earth compounds where localized d- and f-electrons play an important role. One tries to correct the LDA treatment of those orbitals by orbital dependent potentials, i.e. potentials which are nonzero in the atomic spheres only and depend on the orbital state numbers $\ell, m$. This might be the reason for the smaller band gap obtained for $In_2O_3$ using LDA or GGA methods comparing to the experimental values (Hamberg et al., 1984). To solve the problem and obtain the values close to the experimental ones, some workers have shifted the band structures rigidly to higher values, in order to adjust the band gap, by adding a constant to their values (scissors operation). However, we applied LDA+U (instead of LDA or GGA) method with appropriate $U_{eff}$ =U-J for atoms that have localized state such as d-orbital. If the uncorrected LDA approach is used ($U_{eff}$ =0eV), the In 4d state is located at significantly lower binding energies than in experiments value. Increasing the $U_{eff}$ parameter causes to shift the position of the deep In 4d state to more negative binding energies. The LDA+U approach allows us to correct the shortcoming of binding energy for this state.

**Method of Calculations**

The calculations were carried out with a self consistent scheme by solving the Kohn-Sham equations using a FP-LAPW method in the framework of DFT along with the local density approximation (LDA) (Perdew et al., 1992; Peterson et al., 2000) using Wien2k codes (Blaha et al., 2011). The calculation was performed with 1000 k-points and $Rk_{max}$=6 (R is the smallest muffin-tin radius and $k_{max}$ is the cut-off for the plane wave) for the convergence parameter in which the calculations stabilize and convergence in terms of the desired charge e.g. less than 0.001e between steps. The values of the other parameters are $G_{max}$=12 (magnitude of largest vector in charge density Fourier expansion or the plane wave cut-off), the muffin-tin radii for In and O are RMT (In) =2.0 au and RMT (O) =1.6 au, respectively. The cut-off energy, which defines the separation of the valence and core states, was chosen -7 Ry.

In order to calculate the electronic properties of $In_2O_3$ by LDA+U, we assumed that the density matrix is diagonal and U is the same for all Coulomb interactions (Uij≡U) and J is also the same for all exchange interactions (Jij ≡ J). There are several methods to incorporate the U-term (Petukhov et al., 2003; Novak et al., 2006), but here we have used the self-interaction correction (SIC) introduced by Anisimov and coworkers (Anisimov et al., 1993) as implemented in Wien2k package. In the LDA+$U^{SIC}$ methods the total energy may be written as:

The calculations were carried out with a self consistent scheme by solving the Kohn-Sham equations using a FP-LAPW method in the framework of DFT along with the local density approximation (LDA) using Wien2k codes. The calculation was performed with 1000 k-points and $Rk_{max}$=6 ($R$ is the smallest muffin-tin radius and $k_{max}$ is the cut-off for the plane wave) for the convergence parameter in which the calculations stabilize and convergence in terms of the desired charge e.g. less than 0.001e between steps. The values of the other parameters are $G_{max}$=12 (magnitude of largest vector in charge density Fourier expansion or the plane wave cut-off), the muffin-tin radii for In and O are *RMT* (In) =2.0 au and *RMT* (O) =1.6 au, respectively. The cut-off energy, which defines the separation of the valence and core states, was chosen -7 Ry.

$$E = E_0 + E_{LDA+U^{SIC}} \qquad (1)$$

where

$$E_{LDA+U^{SIC}} = \frac{U-J}{2}\left(N - \sum_{m,\sigma} n^2_{m,\sigma}\right) \qquad (2)$$

N is the total number of electrons and nm,σ is the orbital occupancy of the l-orbital in question (i.e. s, p, or d orbital) with spin σ. With an approximated correction value of U-J for the self-interaction correction, this is probably best for a strong correlated system and for a full potential method.
After examining and testing several values of Hubbard potential in order to adjust the In 4d orbital level in the DOS with the experimental value about −15eV as demonstrated in Fig. 1. The final Hubbard potential used in this work was $U_{eff}$=U-J=8.98eV for In atom. The Brillouin zone of $In_2O_3$ with $Ia\bar{3}$ space group (number 206) can be shown either by primitive or conventional as indicated in Fig. 2. In this paper the effective electron mass of $In_2O_3$ and $In_{1.5}$ $T_{0.5}O_3$ (T: Sc, Y, La and Ac) has been calculated for the six directions in the primitive and conventional Brillouin zones. These directions of high symmetry are for primitive and conventional Brillouin zones as follows:

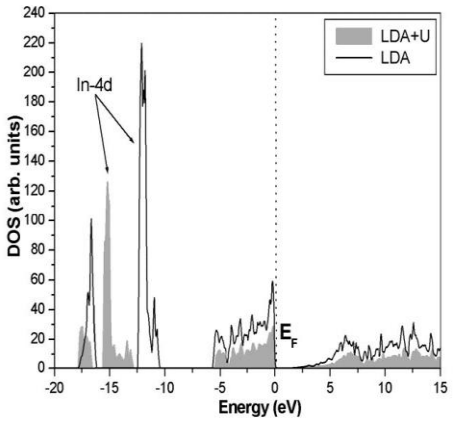


**FIG. 1** **Calculated total density of state of $In_2O_3$ using LDA and LDA+*U*.**

Primitive Brillouin zone:

$\Gamma(0, 0, 0) \rightarrow H\ (1/2, 1/2, 1/2)$
$\Gamma(0, 0, 0) \rightarrow P\ (1/4, 1/4, 1/4)$
$\Gamma(0, 0, 0) \rightarrow N\ (0, 0, 1/2)$

Conventional Brillouin zone:

$\Gamma(0, 0, 0) \rightarrow X\ (1/2, 0, 0)$
$\Gamma(0, 0, 0) \rightarrow M\ (1/2, 1/2, 0)$
$\Gamma(0, 0, 0) \rightarrow R\ (1/2, 1/2, 1/2)$

The diagonal elements of the effective mass tensor, $m_e$, for the electrons in the conduction band were calculated in different directions in $k$ space from the following well-known relations:

$$\frac{1}{m_e(k)} = \frac{1}{\hbar^2}\frac{\partial^2 E(k)}{\partial k^2} \qquad (3)$$

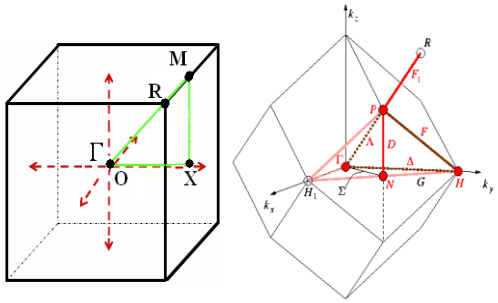


**FIG. 2. (a) Conventional, (b) Primitive Brillouin zone for $In_2O_3$.**

**Structure optimization**

**Lattice parameters**

From the literature, we know that the bulk elastic properties of a material determine how much it will compress under a given amount of external pressure. The ratio of the change in pressure to the fractional volume compression is called the bulk modulus (*B*) of the material and can be written as follows:

$$B = -V\frac{\partial P}{\partial V} \quad (4)$$

In term of energy, the bulk modulus is also defined by equation of state (EOS) and evaluated at the minimum:

$$B = V\frac{\partial^2 E}{\partial V^2} \quad (5)$$

The position of the minimum of EOS defines the equilibrium lattice parameter and unit cell volume at zero pressure. The static lattice potential corresponding to total energy was calculated from a series of strained lattices. From such results the equilibrium volume, bulk modulus and its pressure derivative were derived. A series of total energy calculation as a function of volume can be fitted to an equation of states according to Murnaghan (Murnaghan, 1944):

$$E(V) = E_0 + \frac{B_0 V}{B_0'}\left[\frac{(V_0/V)^{B_0'}}{B_0'} + 1\right] - \frac{B_0 V_0}{B_0' - 1} \quad (6)$$

where $B_0$ is an equilibrium bulk modulus that effectively measures the curvature of the energy versus volume curve about the relaxed volume $V_0$, and $B_0'$ is the derivative of the bulk modulus.

**Atomic relaxation**

Most of structures have free internal structural parameters, which can either be taken from experimental or optimized using the calculated forces on the nuclei. Almost all optimization codes use what is called a quadratic approximation they expand the energy in a form:

$$E^* = E + \mathbf{g}^T\mathbf{s} + (1/2)\mathbf{s}^T\mathbf{H}\mathbf{s} \quad (7)$$

where $E^*$ is the predicted energy for a step ***s*** from the current point, $E$ and ***g*** are the energy and gradient (negative of the force) calculated at the current point and **H** is the Hessian matrix.

Different algorithms use different approaches to the Hessian matrix. The most primitive is steepest descent, which takes **H** as the unitary matrix so will take a step along the direction of the force [38]. For atomic relaxation of $In_2O_3$, we used the reverse-communication trust-region quasi Newton method from the Port library which seems to be stable, efficient and does not depend too much on the user input as implemented in Wien2k package.

**Results and discussion**

**Structure**

Indium oxide can exist in three different phases (Karazhanov et al., 2007) characterized by space group symmetries $I2_13$, $Ia\bar{3}$ and $R\bar{3}$. $In_2O_3$ with space group $Ia\bar{3}$ and the band gap of $Eg$ =3.7 eV is similar to many trivalent rare-earth oxides, such as $Yb_2O_3$ and $Dy_2O_3$. This phase of indium oxide has two non-equivalent six-fold coordinated cation sites, as shown in Fig. 3.

The two cation sites are referred to as equipoints "*b*" and "*d*". The *b* site cations have six equidistant oxygen anion neighbors, which lie approximately at the corners of a cube with two anion structural vacancies along one body diagonal (Wilson, 1992). In this paper the *b* and *d* site cations are referred as cation *I* and *II* with (8a) and (24d) Wyckoff positions, respectively and oxygen's with (48e) Wyckoff positions. The sites of the cations are coordinated to six oxygen anions at three different distances, which lie near the corners of a distorted cube with two empty ions along one face diagonal. The unit cell contains 80 atoms and crystallized in cubic bixbyite structure. The actual unit cell is body centered and contains 8 formula units of $In_2O_3$ with 8 indium atoms at *b* positions, 24 atoms at *d* and 48 oxygen atoms at *e* positions.

Indium oxide can exist in three different phases characterized by space group symmetries $I2_13$, $Ia\bar{3}$ and $R\bar{3}$. $In_2O_3$ with space group $Ia\bar{3}$ and the band gap of $Eg$ =3.7 eV is similar to many trivalent rare-earth oxides, such as $Yb_2O_3$ and $Dy_2O_3$. This phase of indium oxide has two non-equivalent six-fold coordinated cation sites, as shown in Fig. 3.

The two cation sites are referred to as equipoints "*b*" and "*d*". The *b* site cations have six equidistant oxygen anion neighbors, which lie approximately at the corners of a cube with two anion structural vacancies along one body diagonal. In this paper the *b* and *d* site cations are referred as cation *I* and *II* with (8a) and (24d) Wyckoff positions, respectively and oxygen's with (48e) Wyckoff positions.

The sites of the cations are coordinated to six oxygen anions at three different distances, which lie near the corners of a distorted cube with two empty ions along one face diagonal. The unit cell contains 80 atoms and crystallized in cubic bixbyite structure. The actual unit cell is body centered and contains 8 formula units of $In_2O_3$ with 8 indium atoms at *b* positions, 24 atoms at *d* and 48 oxygen atoms at *e* positions.

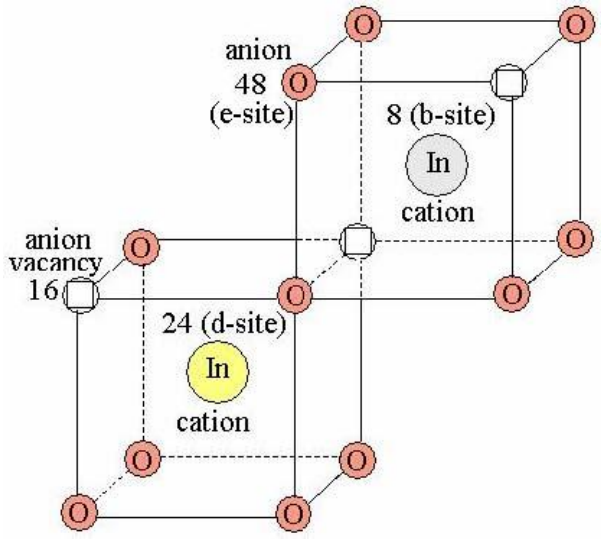


**FIG. 3. Non-equivalent cation sites and anion vacancies in In2O3.**

The calculations were first carried out by applying the experimental data for the lattice constants. Then by minimizing the total energy of the crystal to the volume, the theoretical lattice constants were obtained. The final calculation was performed with the theoretical lattice constant and relaxed structure for $In_2O_3$. The calculated results in this work, and the values obtained by the other methods are summarized in Table 1.

We substituted the impurities in *b* positions, since at low temperatures the impurities prefer to sit at *b* positions. For simplicity, we assume that doping $In_2O_3$ with Sc, Y, La and Ac does not change the symmetries of crystal and we have again the lattice with the same space group ( $Ia\bar{3}$ ). We did minimize the energy for atomic positions and determined the equilibrium position of individual atoms. The final calculation was performed with the theoretical lattice constant and relaxed structure. The results of a full relaxation of anion positions for alloyed $In_{1.5}$ $T_{0.5}O_3$ are given in Table 2. From this table it can be seen that the lattice parameters of $In_{1.5}Sc_{0.5}O_3$ are smaller than $In_2O_3$ due to smaller ionic size of dopant Sc, comparing to In, while Y, La and Ac with larger ionic sizes cause the expansion of the $In_2O_3$ lattice.

### 3.2 Band structure and band gaps

We have calculated the band gaps values of pure $In_2O_3$ and alloyed $In_{1.5}T_{0.5}O_3$ from the band structure as shown in Fig. 4 using LDA+*U* approach. The overall band profiles are calculated in this work is consistent with other first-principles calculation results reported previously. The scale of energy in all figures is in eV and the top of the valence band is set to zero (Fermi level) on the energy scale. The valence bands are separated by a 1.43eV direct gap at *Γ* point from the conduction band states. Experimentally, reported the minimum band gap of $In_2O_3$ to be direct at *Γ* with a value of 3.6eV. Our calculated band gap is smaller than the experimental value but larger than results reported by other first principle approach (table 3). This discrepancy mainly arises from the DFT approximation, which is known to underestimate the energy band gap of semiconductors and insulators. There are two indirect band gaps in the [111] and [110] directions, along *Γ*-*N* and *Γ*-*H*, with a value of 3.47eV and 4.50eV respectively.

**TABLE 1.Calculated lattice parameter and Wyckoff positions for $In_2O_3$ in comparison with experimental and theoretical data.**

| $In_2O_3$ | This work (LDA+*U*) | Experimental (Neutron diffraction) | Theory | Theory |
|---|---|---|---|---|
| Lattice parameter (Å) | 10.057 | 10.121 | 10.117 | 10.077 |
| Cation I (8b) | | | | |
| x | 0.25 | 0.25 | 0.25 | 0.25 |
| y | 0.25 | 0.25 | 0.25 | 0.25 |
| z | 0.25 | 0.25 | 0.25 | 0.25 |
| Cation II (24d) | | | | |
| x | 0.4659 | 0.4660 | 0.4689 | 0.4660 |
| y | 0.0000 | 0.0000 | 0.0000 | 0.0000 |
| z | 0.2500 | 0.2500 | 0.2500 | 0.2500 |
| O (48e) | | | | |
| x | 0.3899 | 0.3900 | 0.38860 | 0.3900 |
| y | 0.1543 | 0.1550 | 0.15167 | 0.1540 |
| z | 0.3821 | 0.3820 | 0.38268 | 0.3820 |

**TABLE 2 Calculated lattice parameter and Wyckoff positions for $In_{1.5}T_{0.5}O_3$.**

| | $In_{1.5}Sc_{0.5}O_3$ | $In_{1.5}Y_{0.5}O_3$ | $In_{1.5}La_{0.5}O_3$ | $In_{1.5}Ac_{0.5}O_3$ |
|---|---|---|---|---|
| Lattice parameter (Å) | 9.987 | 10.187 | 10.446 | 10.546 |
| Cation I (8b) | | | | |
| x | 0.25 | 0.25 | 0.25 | 0.25 |
| y | 0.25 | 0.25 | 0.25 | 0.25 |
| z | 0.25 | 0.25 | 0.25 | 0.25 |
| Cation II (24d) | | | | |
| x | 0.4653 | 0.4668 | 0.4725 | 0.4779 |
| y | 0.0000 | 0.0000 | 0.0000 | 0.0000 |
| z | 0.2500 | 0.2500 | 0.2500 | 0.2500 |
| O (48e) | | | | |
| x | 0.3876 | 0.3929 | 0.4003 | 0.4061 |
| y | 0.1580 | 0.1522 | 0.1438 | 0.1391 |
| z | 0.3811 | 0.3843 | 0.3835 | 0.3805 |

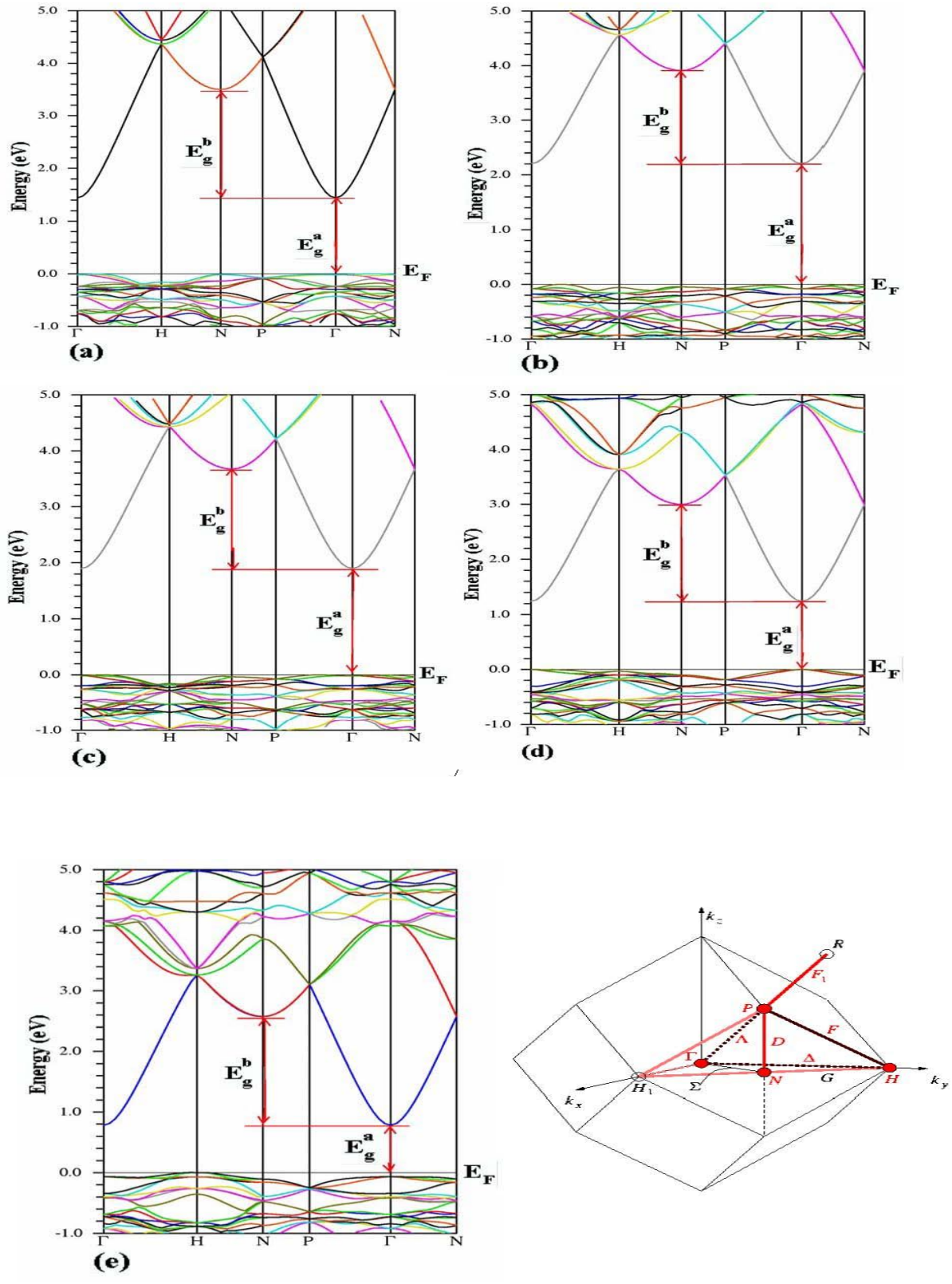


**FIG. 5 A portion of band structure for $In_2O_3$.**

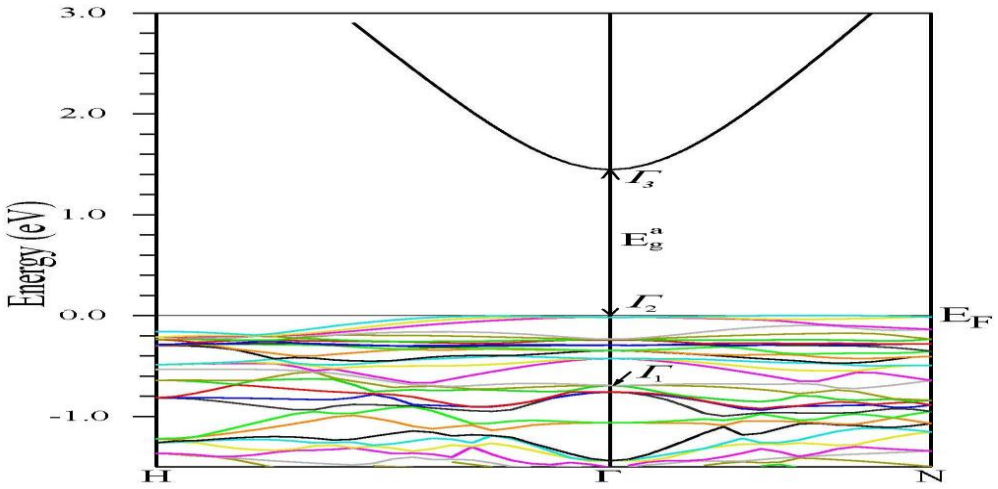


**TABLE 3. Calculated band gaps values for $In_2O_3$ and alloyed $In_{1.5}Ti_{0.5}O_3$.**

| Band gap (eV) | $E_g^a$ | $E_g^b$ | $\Gamma_1 \rightarrow \Gamma_2$ | $\Gamma_2 \rightarrow \Gamma_3$ | $\Gamma_1 \rightarrow \Gamma_3$ |
|---|---|---|---|---|---|
| This work: (FL-LAPW method GGA | | | | | |
| $In_2O_3$ | 1.43 | 2.04 | 0.78 | 1.43 | 2.21 |
| $In_{1.5}Sc_{0.5}O_3$ | 2.18 | 1.68 | – | – | – |
| $In_{1.5}Y_{0.5}O_3$ | 1.88 | 1.76 | – | – | – |
| $In_{1.5}La_{0.5}O_3$ | 1.24 | 1.76 | – | – | – |
| $In_{1.5}Ac_{0.5}O_3$ | 0.82 | 1.80 | – | – | – |
| Theory: | | | | | |
| LDA [19] | | | | | |
| $In_2O_3$ | 1.10 | 2.86 | – | – | – |
| GGA [18] | | | | | |
| $In_2O_3$ | 1.03 | 1.77 | – | – | – |
| LMTO [21] | | | | | |
| $In_2O_3$ | 1.0 | – | – | – | – |
| Experimental | | | | | |
| $In_2O_3$ Thin film [45] | – | – | – | – | 3.27 |
| $In_2O_3$ Bulk [51, 52] | – | – | 0.82 | 2.62 | 3.75 |

**Band structure and band gaps**

The calculated energy gapes for $In_2O_3$, $In_{1.5}Sc_{0.5}O_3$, $In_{1.5}Y_{0.5}O_3$, $In_{1.5}La_{0.5}O_3$ and $In_{1.5}Ac_{0.5}O_3$ are 1.43, 2.18, 1.88, 1.24 and 0.82eV respectively which indicates that the substitution of Sc and Y atoms for In has increased the band gap and substitution of La and Ac atoms for In has decreased the band gap significantly.

As indicated by J. E. Medvedeva the widening of band gap may appear from the anisotropic *d* orbitals of Sc and Y which rotate the *p* orbitals of the neighboring oxygen. Then the overlap of these *p* orbitals with In *5s* state in the bottom of the conduction band increases, and hence leading to the widening of the band gap. The narrowing of band gap for impurities of La and Ac is a consequence of many body effects on the conduction band and that can also be altered by reduction of lattice parameters and the local strains induced by these impurities.

**Effective mass**

The electron effective mass for pure and the alloys of $In_2O_3$ are obtained from the curvature of the conduction band at $\Gamma$ point. To illustrate how the alloying by transition metals alter the electronic band structure of the host material, we have enlarged the band structures of pure $In_2O_3$ and alloyed with Sc, Y, La and Ac as illustrated in Fig. 6. The bottom of the conduction band structure for two directions $\Gamma \rightarrow X$ and $\Gamma \rightarrow H$ has been plotted. The electron effective mass has been determined from fitting the electronic band structure to a parabolic function (equation 3) for the six directions in the first Brillouin zone using LDA+*U* approaches. The values of calculated electron effective mass for $In_2O_3$ in $\Gamma \rightarrow X$, $\Gamma \rightarrow M$ and $\Gamma \rightarrow R$ directions are 0.374*me*, 0.386*me*, 0.391*me* respectively and also for the $\Gamma \rightarrow H$, $\Gamma \rightarrow P$and $\Gamma \rightarrow N$ directions are 0.400*me*, 0.391*me* and 0.419*me* respectively. The corresponding values for pure $In_2O_3$, alloys of $In_{1.5}$ $T_{0.5}O_3$, pure $Cd_3TeO_6$ and doped with In obtained by the others are also summarized in the table 4. The effective free electron masses determined by GGA approach as a function of doping element for three directions in the Brilluoin zone are shown in table 4. The results indicated that the while the band gap values sensitive to the values of Hubbard potential (*U*) but the effective electron masses are not. Overall the effective free electron mass did not change more than about 0.02me units for LDA+*U* and GGA approach. $^{*}Cd_3TeO_6$ substituted with In in B-site. The ternary oxide $Cd_3TeO_6$ has a deformed perovskite-type structure (monoclinic, $P2_1/n$) in which B sites are occupied by $Cd^{2+}$ and $Te^{6+}$ ions in a ratio of 1:1 and A sites are filled solely by $Cd^{2+}$ ions. The value of the electron effective mass in the conduction band is increased in all the six directions for alloys $In_2O_3$, so the mobility of electrons is decreased in these directions. The increase of the electron effective mass in indium oxide alloys with Ac is less than that for Sc, Y and La.

**Density of states (DOS)**

The results of density of states calculation show that the main contribution to the top of the valence band comes from Sc *3d*, Y *4d*, La *5*d, Ac *6d* and O *2p* atomic orbitals as indicated in Fig. 7. The bottom of the conduction band is mainly formed from In *5s* hybridized with O *2s* orbitals, although the conduction band has contributions from all atoms. For $In_2O_3$, the high dispersion and s-type character in the bottom of the conduction band may also explain high conductivity, as a result of high mobility of these states. The s-type character of this band results in an isotropic distribution of the electronic charge density and relatively low scattering.

**FIG. 6. The calculated bands at the bottom of the conduction band using LDA+*U* for In2O3, In1.5Sc0.5O3, In1.5Y0.5O3, In1.5La0.5O3 and In1.5Ac0.5O3 in (a) Γ→*X* (b) Γ→*H*.**

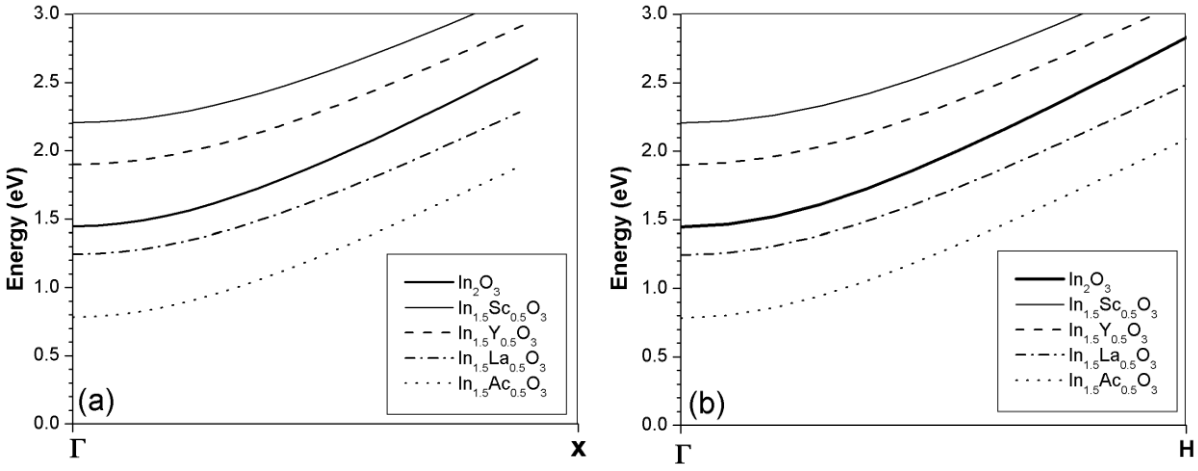


**TABLE 4. Calculated electron effective mass in the conduction band with LDA+*U* approaches for $In_2O_3$ and $In_{1.5}T_{0.5}O_3$ (T=Sc, Y, La, and Ac).**

| Directions | Γ→X | Γ→M | Γ→R | Γ→H | Γ→P | Γ→N |
|---|---|---|---|---|---|---|
| This work: (FL-LAPW method GGA) | | | | | | |
| $In_2O_3$ | 0.380$m_e$ | 0.385$m_e$ | 0.387 $m_e$ | 0.397$m_e$ | 0.387$m_e$ | 0.415$m_e$ |
| $In_{1.5}Sc_{0.5}O_3$ | 0.538$m_e$ | 0.543$m_e$ | 0.550$m_e$ | 0.556$m_e$ | 0.550$m_e$ | 0.572$m_e$ |
| $In_{1.5}Y_{0.5}O_3$ | 0.488$m_e$ | 0.498$m_e$ | 0.507$m_e$ | 0.514$m_e$ | 0.507$m_e$ | 0.529$m_e$ |
| $In_{1.5}La_{0.5}O_3$ | 0.466$m_e$ | 0.468$m_e$ | 0.474$m_e$ | 0.480$m_e$ | 0.474$m_e$ | 0.499$m_e$ |
| $In_{1.5}Ac_{0.5}O_3$ | 0.400$m_e$ | 0.400$m_e$ | 0.404$m_e$ | 0.411$m_e$ | 0.404$m_e$ | 0.433$m_e$ |
| This work: (FL-LAPW method LDA+U) | | | | | | |
| $In_2O_3$ | 0.374$m_e$ | 0.386$m_e$ | 0.391 $m_e$ | 0.400$m_e$ | 0.391$m_e$ | 0.419$m_e$ |
| $In_{1.5}Sc_{0.5}O_3$ | 0.457$m_e$ | 0.490$m_e$ | 0.510$m_e$ | 0.514$m_e$ | 0.510$m_e$ | 0.547$m_e$ |
| $In_{1.5}Y_{0.5}O_3$ | 0.475$m_e$ | 0.469$m_e$ | 0.476$m_e$ | 0.484$m_e$ | 0.476$m_e$ | 0.507$m_e$ |
| $In_{1.5}La_{0.5}O_3$ | 0.420$m_e$ | 0.438$m_e$ | 0.444$m_e$ | 0.453$m_e$ | 0.444$m_e$ | 0.467$m_e$ |
| $In_{1.5}Ac_{0.5}O_3$ | 0.383$m_e$ | 0.387$m_e$ | 0.394$m_e$ | 0.402$m_e$ | 0.394$m_e$ | 0.428$m_e$ |
| Theory: | | | | | | |
| $In_2O_3$ (quantum chemical software) DMol3 [23] | | | | | | |

| | | | | | | |
|---|---|---|---|---|---|---|
| | 0.300$m_e$ | 0.360$m_e$ | 0.410$m_e$ | – | – | – |
| $In_2O_3$ ( GGA+*U*) [19] | – | – | – | 0.230$m_e$ | 0.230$m_e$ | 0.200$m_e$ |
| $In_2O_3$ (tight-binding linear muffin-tin orbital ) LMTO method [21] | | | | | | |
| | – | – | – | 0.420$m_e$ | 0.300$m_e$ | 0.360$m_e$ |
| $In_{30}Sn_2O_{48}$ (quantum chemical software) DMol3 [23] | | | | | | |
| | 0.320$m_e$ | 0.470$m_e$ | 0.640$m_e$ | – | – | – |
| $Cd_3TeO_6$(FLAPW method, GGA)[44] | | | | | | |
| | 0.206 $m_e$ | 0.210 $m_e$ | 0.214 $m_e$ | – | – | – |
| $Cd_3TeO_6$(FLAPW method, GGA)[44]* | | | | | | |
| | 0.291 $m_e$ | 0.293 $m_e$ | 0.309 $m_e$ | – | – | – |
| Experimental: | | | | | | |
| Sn doped $In_2O_3$ [28] | – | – | – | – | 0.300$m_e$ | – |
| $In_2O_3$ (thin films) [46] | – | – | – | – | 0.31$m_e$ to 0.43$m_e$ | – |

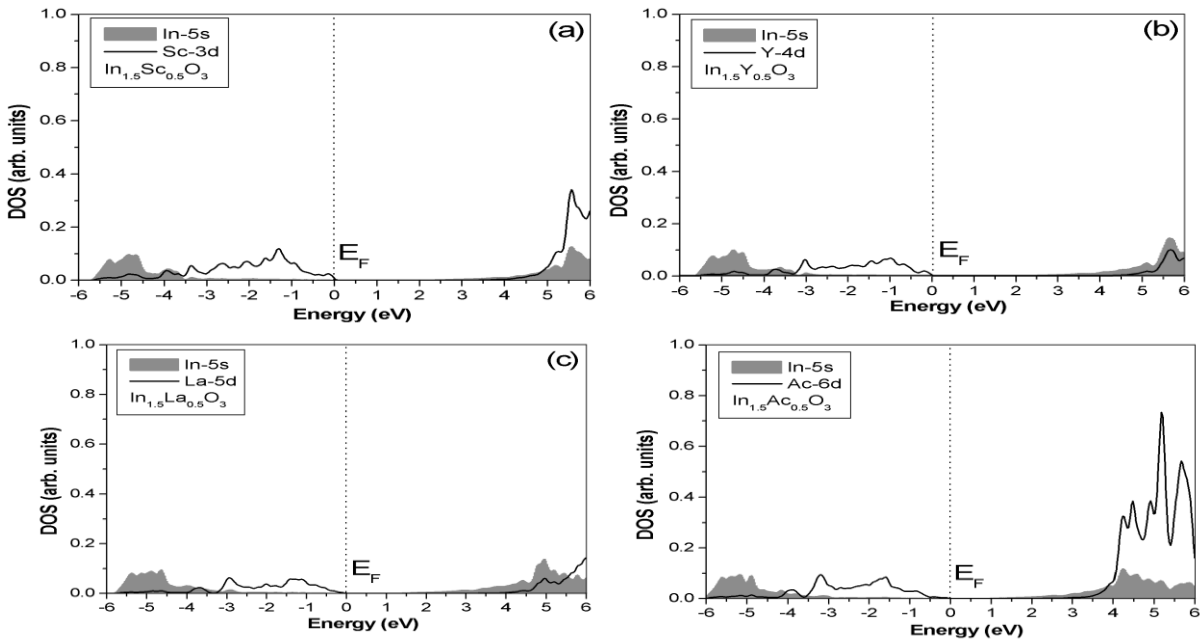


**FIG. 7. Calculated DOS using LDA+*U* approach for (a) Sc *3d* and In *5s* in $In_{1.5}Sc_{0.5}O_3$, (b) Y *4d* and In *5s* in $In_{1.5}Y_{0.5}O_3$ , (c) La *5d* and In *5s* in $In_{1.5}La_{0.5}O_3$ and (d) Ac *6d* and In *5s* in $In_{1.5}Ac_{0.5}O_3$.**

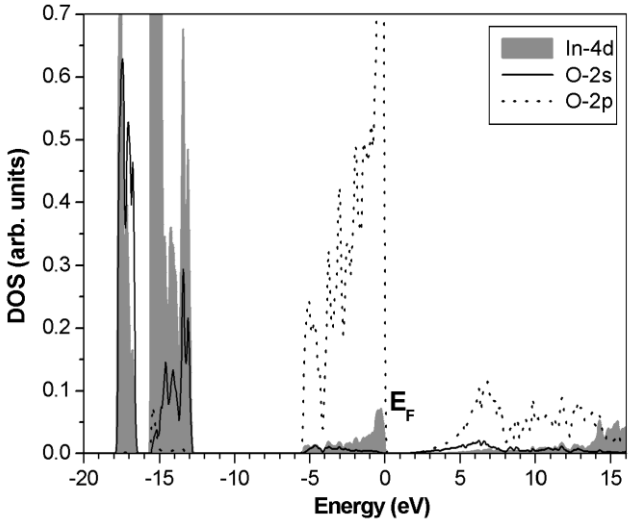


**FIG. 8. Calculated partial density of states using LDA+*U* for $In_2O_3$.**

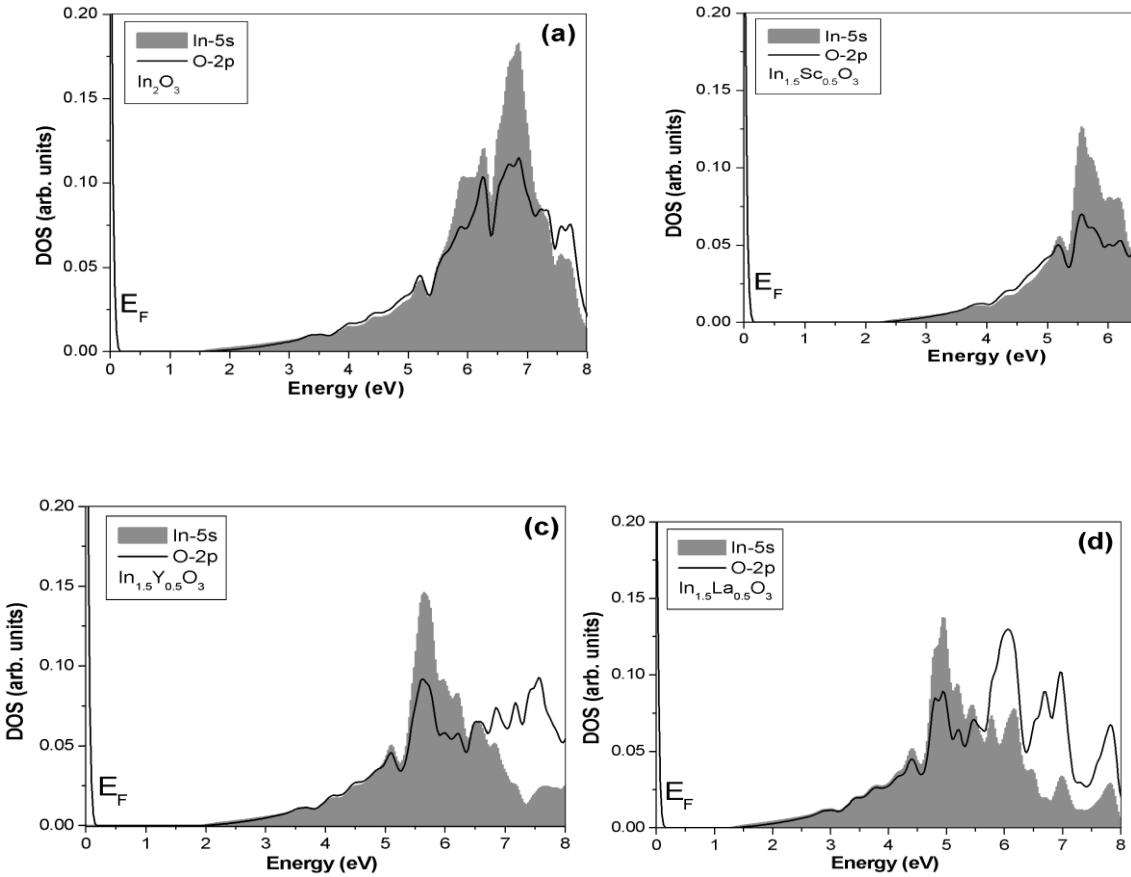

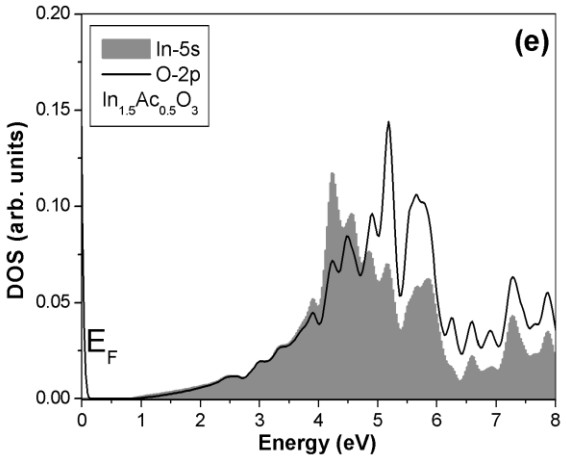


**FIG. 9. Calculated partial density of states using LDA+*U* for In *5s* and O *2p* for (a) $In_2O_3$, (b) $In_{1.5}Sc_{0.5}O_3$, (c) $In_{1.5}Y_{0.5}O_3$ , (d) $In_{1.5}La_{0.5}O_3$ and (e) $In_{1.5}Ac_{0.5}O_3$.**

The energetic position of In *4d* state of $In_2O_3$, however, affects the hybridization of In *4d* with O *2s* and O *2p* orbital, as shown in Fig. 8. In addition, while the In *4d*, O *2p* mixing is reduced, the In *4d*, O *2s* hybridization increases. Regarding the In-O interaction, as indicated by I. Tanaka *et al*. from overlap-population diagrams the major part O *2s* band is completely bonding and the In *4d* band displays both bonding and antibonding contributions for almost the same amount. Due to the interaction between O-2*p* and In-4*d* orbitals near the top of the valence band there is also an antibonding contribution. The O-O bond is less significant than the In-O bond. The In-In interaction is much weaker than the other two kinds of bonds. These kinds of interactions have been also observed experimentally by Barr and Liu using x-ray photoelectron spectroscopy (XPS).

Results of DOS calculation also yielded some information concerning the conduction bands of $In_2O_3$, $In_{1.5}Sc_{0.5}O_3$, $In_{1.5}Y_{0.5}O_3$, $In_{1.5}La_{0.5}O_3$ and $In_{1.5}Ac_{0.5}O_3$. The Sc *4*s, Y *5*s, La *6s* and Ac *7s* states are found to lie high in the conduction band and thus do not hybridize with the In *5s* states, as indicated in Fig. 9. where the *d*-orbitals of the dopant ions hybridize only with the *p*-orbitals of the nearest oxygen neighbors

**The effect of dopant ionic radius**

The calculated results indicated that the electronic structure and ionic radii of dopants have a significant influence on the electronic properties of $In_2O_3$ crystals. It is found that smaller dopant ionic radius results in weaker In *5s* and O *2p* hybridization due to the relaxation of the oxide anions around the dopant cations. Therefore, any expanding in the lattice parameter, due to the larger Y, La and Ac ions, is well compensated by the antibonding expansion mechanism, in contrast to Sc-alloys of $In_2O_3$ where the lattice is significantly compressed due to the very much smaller ionic radius of Sc, leading to inducing the diminished *s-p* hybridization between In *5s* and O *2*p orbitals as indicated in Fig. 10. Yu Yang *etal.* have doped CdO with the In, Sc, and Y and found that dopant ion size and electronic configuration have substantial influence on the CdO-based TCOs crystal and band structure, especially on the energetic position and width of the highly dispersed conduction band, which provide necessary conditions for creating transparent conducting behavior with doping. Therefore, the uniform electronic charge density distribution is not possible in the Sc, Y, La and Ac cases. They have reported also Y doping of CdO widens the optical band gap and doping with Sc (smaller dopant ionic radii) result in weaker Cd *5s*-O *2p* hybridization due to relaxation of the oxide anions around the dopant cations.

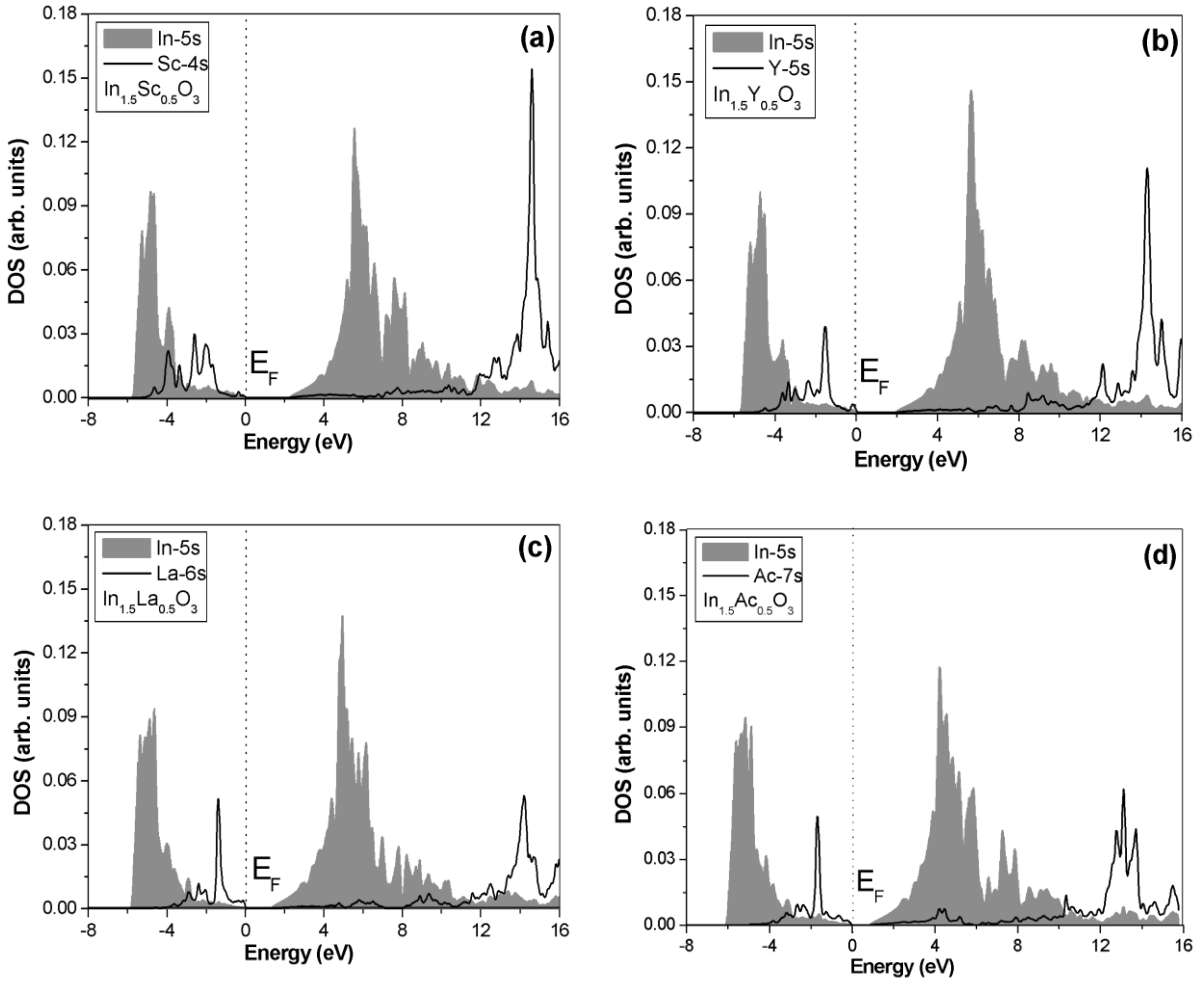


**FIG. 10. Calculated partial density of states using LDA+*U* for (a) In *5s* and Sc *4s* in $In_{1.5}Sc_{0.5}O_3$, (b) In *5s* and Y *5s* in $In_{1.5}Y_{0.5}O_3$ (c) In *5s* and La *6s* in $In_{1.5}La_{0.5}O_3$ and (d) In *5s* and Ac *7s* in $In_{1.5}Ac_{0.5}O_3$.**

However, our results of calculation and the effect of doped on electronic properties of $In_2O_3$ are consistent with the theoretical and experimental results reported for Sc, Y and In doped CdO-based TCOs thin films and bulk materials.

**Conclusions**

In this work we have studied structural and electronic properties of $In_2O_3$ and alloyed $In_{1.5}T_{0.5}O_3$ (T: Sc, Y, La, Ac) namely: the effect of dopant ionic size on the lattice parameters, Wyckoff positions of the atoms, the effective electron mass, the band gaps, and the conduction band orbital character, using DFT calculations with LDA+*U*. It is found that doping of Sc in $In_2O_3$ shrinks the lattice while the other three dopants expand the lattice, due to their ionic sizes. These shrinkage and expansion of the lattice change affect the band structure and hence the band gap value.

We calculated the electron effective mass for pure and alloys $In_2O_3$ in the primitive and conventional Brillouin zone. Our results show that for alloys $In_2O_3$ the value of the electron effective mass in the

conduction band has increased along the six directions, resulting in the decrease of the mobility of electrons. The calculated band structure revealed that the lowest conduction band of $In_2O_3$ is formed from a highly dispersed single In *5s* orbital, and the top of the valence band comes from the O *2p* orbital. The results indicate that the ionic sizes of the dopants and their electronic configuration have significant influence on structural and electronic properties of $In_2O_3$-based TCO crystals. It is found that the properties of $In_2O_3$ alloy depends strongly on the degree of orbital hybridization between the dopant orbital and In *5s* states. Also our results show that In *5s* states do not have significant hybridization with Sc *4s*, Y *5s*, La *6s* and Ac *7s* states

**Acknowledgements**

The authors are grateful to Professor P. Blaha (at Vienna University of Technology Austria) for his technical assistance in using Wien2k codes.

**References**

**Anisimov VI, Solovyev IV, Korotin MA, Czyzyk MT, Sawatzky GA (1993)** "Density-functional theory and NiO photoemission spectra". Phys. Rev. B, Vol. 48, No. 23, pp. 16929-16934.

**Blaha P, Schwarz K, Madsen G, Kvasnicka D, Luitz J (2011)** "Institute of Mater. Chem.TU Vienna", http://www.wien2k.at/.

**Bilbao crystallographic server: (2011)** "The crystallographic site at the Condensed Matter Physics Department of the University of the Basque Country". http://www.cryst.ehu.es/.

**Coutts TJ, Perkins JD, Ginley DS, Mason TO (1999)** "Transparent Conducting Oxides: Status and Opportunities in Basic Research. Presented at the 195th Meeting of the Electrochemical Society", Seattle, Washington May 2-6.

**Coutts TJ, Young DL, Li X (2000)** "Characterization of transparent conducting oxides". MRS Bulletin, Vol. 25, No. 55, pp. 58-65.

**Dou Y, Egdell RG, Walker T, Law DSL, Beamson G(1998)** "N-type doping in CdO ceramics: A study by EELS and photoemission spectroscopy". Surf. Sci., Vol. 398, No.12, pp. 241-258.

**Ginley DS, Bright C (2000)** "Transparent Conducting Oxides". MRS Bulletin, 15-18, August. http/www.mrs.org/publications/bulletin/.

**Ginley DS, Taylor MP, Van Hest MFAM, Young D, Teplin CW, Alleman JL, Dabney MS, Parilla P, Gedvilas LM, Keyes BM, To B, Readey D, Perkins JD (2005)** "Combinatorial Exploration of Novel Transparent Conducting Oxide Materials". Solar Energy Technologies Program Review Meeting, Denver, Colorado, USA.

**Gonzalez GB, Cohen JB, Hwang JH, Mason TO, Hodges JP, Jorgensen JD (2001)** "Neutron diffraction study on the defect structure of indium–tin–oxide". J. Appl. Phys., Vol. 89, No.43, pp. 2550-2555.

**Hayashi K, Sushko PV, Shluger AL, Hirano M, Hosono H (2005)** "Hydride Ion as a Two-Electron Donor in a Nanoporous Crystalline Semiconductor 12CaO.7Al2O3". J. Phys. Chem. B,Vol. 109, No. 21, pp. 36-42.

**Hamberg I, Granqvist CG, Berggren KF, Sernelius BE, EngstrÖm L (1984).** "Band- gap widening in heavily Sn-doped $In_2O_{3-}$". Phys. Rev. B., Vol. 30, No.11, pp. 3240-3249.

**Kajihara K, Matsuishi S, Hayashi K, Hirano M, Hosono H (2007)** "Vibrational Dynamics and Oxygen Diffusion in a Nanoporous Oxide Ion Conductor 12CaO.7Al2O3 Studied by 18O Labeling and Micro-Raman Spectroscopy". J. Phys.Chem. C, Vol. 111, No. 12, pp. 55-61.

**Karazhanov SZ, Ravindran P, Vajeeston P, Ulyashin A, Finstad TG, Fjellvag H (2007)** "Phase stability, electronic structure and optical properties of indium oxide polytypes". Phys. Rev. B., Vol. 76, No. 45, pp. 1291-1313.

**Klein A (2000)** "Electronic properties of $In_2O_3$ surfaces". Appl. Phys. Lett., Vol. 77, No. 9, pp. 2009-2011.

**Kompany A, Rahnamaye Aliabad HA, Hosseini SM (2007)** "Effect of substituted IIIB transition metals on electronic properties of Indium Oxide by first-principle calculations". Phys. stat. sol. B., Vol. 244, No. 21, pp. 619-628.

**Lewis NG, Paine DC (2000) "**Applications and Processing of Transparent Conducting Oxides". MRS Bulletin- Materials Research Society, Vol. 25, No.4, pp. 22-27.

**Lo S S, Lin CY, Jan DJ (2011)** "Transparent conductive oxide layer with monolayer closed-pack Al-doped ZnO spheres and their application to a-Si thin-film solar cells". Opt. Lett., Vol. 36, No.8, pp. 3678-3680.

**Matsuishi S, Toda Y, Miyakawa M, Hayashi K, Kamiya T, Hirano M, Tanaka I, Hosono H (2003)** "High-Density Electron Anions in a Nanoporous Single Crystal: $[Ca_{24}Al_{28}O_{64}]4+$ (4e-)". Science, Vol. 301, No.3, pp. 626-29.

**Minami T (2005) "**Transparent conducting oxide semiconductors for transparent electrodes". Semicond. Sci. Technol., Vol. **20, No.6**, pp. S35-S44.

**Medvedeva JE, Freeman AJ (2005)** "Combining high conductivity with complete optical transparency: A band structure approach" Europhys. Lett., Vol. 69, No.8, pp. 583-587.

**Medvedeva JE (2006) "**Magnetically Mediated Transparent Conductors: $In_2O_3$ Doped with Mo". Phys. Rev. Lett., Vol. 97, No.1, pp. 111-114.

**Mott NF (1987)** "Conduction in non-crystalline materials", 1st ed. Oxford Science Publications, Oxford.

**Murnaghan FD (1944)** "The Compressibility of media under extreme pressures", Proceedings of the National Academy of Sciences,, Vol. **30, No.3,** pp. 244-247.

**Noginov MA, Gu L, Livenere J, Zhu G, Pradhan AK, Mundle R, Bahoura M, Barnakov YA, Podolskiy VA (2011)** "Transparent conductive oxides: Plasmonic materials for telecom wavelengths". Appl. Phys. Lett., Vol. 99, No. 33, pp. 101-109.

**Novak P, Kunes J, Chaput L, Pickett WE (2006)** "Exact exchange for correlated electrons". Phys. Stat. Sol. B., Vol. 243, No.13, pp. 563-572.

**Ott AW, Chang RPH (1999)** "Atomic layer-controlled growth of transparent conducting ZnO on plastic substrates". Materials Chemistry and Physics., Vol. 58, No.24, pp. 132-138.

**Ohsawa T, Okubo J, Suzuki T, Kumigashira H, Oshima M, Hitosugi T (2011)** "An n-Type Transparent Conducting Oxide: $Nb_{12}O_{29.}$ J. Phys. Chem. C, Vol. 115, No.104, pp. 16625–16629.

**Perdew JP, Chevary JA, Vosko SH, Jackson KA, Pederson MR, Singh DJ, Fiolhais C (1992)** "Atoms, molecules, solids, and surfaces: applications of the generalized gradient approximation for exchange and correlation". Phys. Rev. B **46, No.76,** pp. 6671-6687.

**Peterson M, Wanger F, Hufnagel L, Scheffler M, Blaha P, Schwarz K (2000)** "Improving the efficiency of FP-LAPW calculations.Compute". Phys. Commun., Vol. 126, No.3, pp. 294-309.

**Petukhov AG, Mazin II (2003)** "Correlated metals and the LDA+U method". Phys. Rev. B., Vol. 67, No. 43, pp. 231-237.

**Phillips JM, Cava RJ, Carter SA, Kwo J, Hou SY, Krajewski JJ, Marshall JH, Peck WF , Rapkine DH (1995)** "A highly-conducting transparent conductor: Zinc Indium Tin Oxide". Appl. Phys. Lett., Vol. 67, No.14, pp. 2246-2248.